MEASUREMENT OF RESULTANT ACCELERATION UTILIZING A WEIGHT BALL ROLLING IN A SPHERICAL SHELL

Tokuji Okada [1], Ken-ichi Kurosaki[1], Karsten Berns[2], Ruediger Dillmann[3]

[1]Faculty of Engineering, Niigata University, Japan
[2]Forschung Zentrum Informatik, Karlsruhe University, Germany
[3]Institute for Real-time Computer systems and Robotics, Karlsruhe University, Germany

ABSTRACT

This paper describes measurement of resultant acceleration of motion and gravity in 3D space based on sensing a metallic ball position on elastic layer housed in a spherical shell. Construction of different types of silicon rubber is introduced and their displacements against pressure are calculated by using the Hertz' law. Since the resultant acceleration makes the ball roll toward the direction to find a balanced position in the shell, the center position of the metallic ball is measured. The rubber layer is concentric to the shell and liable to distort so that three proximity sensors of high-frequency oscillation type can detect characteristics of sink versus pressure. We show measurement principle of extracting the acceleration by using the characteristics. Experimental results are shown and compared among various rubbers to have the most appropriate design of the sensor. We got practical data such that angular error less than $\pm$ 7.4[deg]; amount error less than 2.86 x 10^{-2} [m/s^2]; force sensitivity 4.9 x 10^{-2}[N]; insensible range less than $\pm$ 3.8[deg]; periodic time 95[ms].

1. INTRODUCTION

Progress of manufacturing integrated circuits made it possible to fabricate small sized solid sensors, devices attaching a resonator for sensing force and weight [1], [2], [3]. Nowadays, an IC chip-sized device for sensing acceleration is commercially available [4]. However, most of them are designed for the use in limited range of motion around a specific axis. Therefore, they have such features that 1) the shaft like a pendulum is not free from friction generated at its bearing stand. This friction disturbs improvement of sensitivity and resolution, 2) unification of several sensing elements is difficult to make the device smart, and 3) the measurement accuracy is not always unique in overall directions. In the device using rotation media of a float or liquid, 4) surface tension or free deformation of the media becomes noise. 5) Measurement error accumulates as time passes in such gyroscopes using inertia of a rotor, time difference or phase difference of optical propagation, and 6) the gyroscope is expensive to use in practical applications. These weak points seem to be caused by partial and individual make-up of sensing mechanism and collection of electric signals

To solve the above-mentioned weak points, we make-up a sensor head with a ball and shell so that the ball can roll freely along interior wall of the shell. Three proximity sensors of high frequency oscillation type are located at exterior of the shell. Outputs of these sensors are unified to find center position of the ball [5]. Evidently, ball positions are principal information to determine acceleration operating on the shell. Based on this knowledge, the ball is a heavy mass and interior of the shell is uniquely covered with an elastic layer. Also, the layer might envelop the ball. Actually, the ball distorts the layer to sink, and the amount of sink is determined since the ball position is settled including the sink and the compliant characteristics of the layer is clarified in advance. That is, the direction of the ball existing from the center of the shell expresses the direction of acceleration, and the force operating on the ball divided by the mass expresses the amount of acceleration.

This paper describes the relationship between depression versus load on elastic layers, fabrication of elastic layers and assembly of the device as a sensor head. In the analysis of clarifying the relationship between depression versus pressure of the elastic layers, we suppose

two spring models to get mathematical expressions and prove validity of them by comparing analytical and experimental result [5]. Experimental results obtained in static condition show that the proposed acceleration measurement is quite useful since sensing mechanism and signal processing is simple.

2. PHYSICAL PROPERTIES OF A SPHERICAL ELASTIC LAYER

2.1 Hertz' law

When a spherically-formed indenter presses an flat layer, depression appears on the flat material and related analytical equations are found in [6], [7]. Most of the analyses are carried between two different objects in shape but either object is almost assumed to be flat. The depression is estimated in an ideal case such that spherically convex and concave objects extend indefinitely toward inside and outside, respectively (see Fig.1). Let suppose that subscripts 1 and 2 identify the two objects, and that the symbols r, E, ν, σ and δ stand for radius, Young's modulus, Poisson's ratio, load (pressure) and maximal depression, respectively. Then, the equation is given by [8]

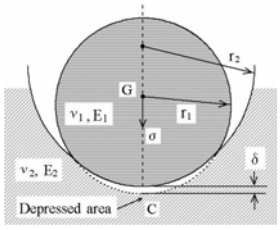

Figure1: Objects' contact

$$\delta^3 = \frac{9}{16}\frac{r_2 - r_1}{r_1 r_2}\left(\frac{1-\nu_1^2}{E_1} + \frac{1-\nu_2^2}{E_2}\right)^2 \sigma^2 \qquad (1)$$

Since the aim of our layer is to sense the force operating to the metallic ball, two contacting objects do not need to be elastic together. Also, it is recommended to make sensing mechanism and signal processing simple. Thus, combination of the two elastic objects is not our subject. Our combination is either of the two shown in Fig.2. The ball is naked to be rigid and interior of the shell is covered with elastic layer in (a). The composition in (b) is opposite. We name the two compositions *rigid ball type* and *elastic ball type*, respectively. In both compositions some of the parameters become constant (see Fig.3) since our rigid object is made of iron, that is, E=1.96x10^3[Pa], ν=0.31 [9]. These physical constants simplify the expression (1) as follows

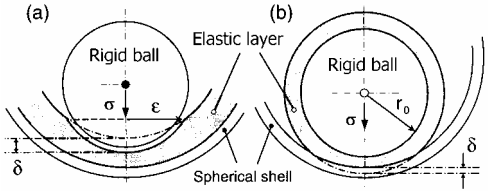

Figure2: Two composition types of the layer

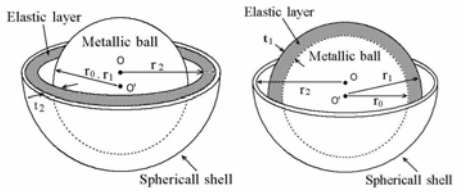

Figure3: Parameters of the two assembly types

$$\delta^3 = \frac{9}{16}\frac{r_2 - r_1}{r_1 r_2}\left(3.824\times10^{-4} + \frac{1-\nu_r^2}{E_r}\right)^2 \sigma^2 \qquad (2)$$

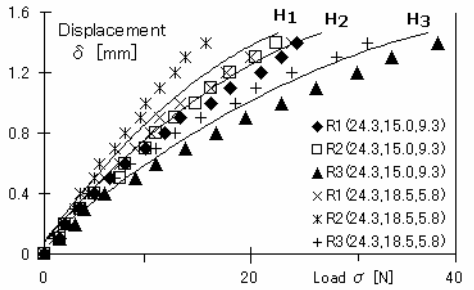

Figure4: σ versus δ characteristics of R_1, R_2, R_3

The rigid ball type has the elastic layer of thickness t_2 contacting with the shell of radius r_2+t_2 in a concentric configuration. The elastic ball type has the layer of thickness t_1 to envelop the ball to make observed radius $r_1=r_0+t_1$ in a concentric configuration.

Equation (2) seems to be valid when the layer is thick enough, but we need to confirm in fact. Therefore, we made elastic test pieces of t_2=5.8[mm] (r_2=18.5[mm]) and 9.3[mm] (r_2=15[mm]) as the rigid ball type of r_1=12.7[mm] and r_2+t_2=24.3[mm]. In Fig.4, experimental data on δ versus σ characteristics are compared with the data calculated by the equation (2) under r_1=12.7[mm]. Symbols ", x, ', *, %, + show the results of different test pieces in sizes which we express by Rn (B_1, B_2, B_3), where B_1, B_2 and B_3 mean outer diameter, inner diameter and

thickness of the layer in mm dimension. Symbols H_1, H_2 and H_3 mean difference in layer material. Actually, the data identified by H_1, H_2 and H_3 are calculated under r_2 is 16.75[mm] {=(18.5+15.0)/2} and combination (ν_r, E_r) of (0.50, 1.1[Pa]), (0.50, 1.3[Pa]) and (0.50, 1.8[Pa]), respectively [9]. Detailed make-up and measurement of the elastic material are described in section 3. From the figure 4, it is evident that sensitivities of the data x, *, + are higher than those of the data ", ', %. Also, the thick layered data x, ', + are closer to the analytical data of H_1, H_2, H_3, respectively. These facts show delicacy of δ versus σ characteristics around the data calculated by equation (2).

2.2 Modeling of an elastic layer by springs

We analyze the δ versus σ characteristics of the rigid ball type by introducing spring models. We define spring coefficient k as a function of t_2 expressing the thickness of the elastic layer.

$$k = u E_r / t_2 \qquad (3)$$

where u is a constant.

2.2.1 Array of radial spring alignment

Notice that the section including maximal depression of the layer is shown in Fig.5 and the contact point of the ball with the elastic layer is within circumferential circle of radius a. Then, the total load σ is found as follows

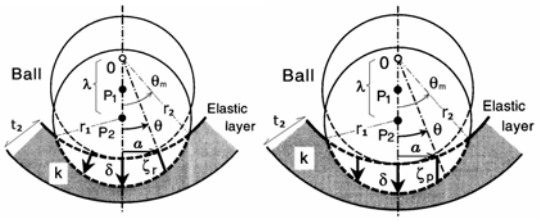

Figure5: Two spring models of the elastic layer

$$a = r_2 \sin\theta \qquad (4)$$

$$\zeta_r = -(r_2 - \lambda\cos\theta) + (r_1^2 - \lambda^2 \sin^2\theta)^{1/2} \qquad (5)$$

$$\sigma = \int_0^{\theta_m} 2\pi\, a\, k\, \zeta_r \cos\theta \, \mathrm{d}\theta \qquad (6)$$

$$\theta_m = \cos^{-1}\{(r_2^2 - r_1^2 + \lambda^2)/(2\lambda r_2)\} \qquad (7)$$

where $\lambda = r_2 - r_1 + \delta$ (8)

Finally, inserting (3)-(5), (7),(8) to (6) yields

$$\sigma = \frac{\pi u r_2 E_r}{12 t_2}\left[24\delta(1-\cos\theta_m) - r_2^2(1/r_1 - 1/r_2)\{-9\cos\theta_m + \cos(3\theta_m) + 8\}\right] \qquad (9)$$

2.2.2 Array of parallel spring alignment

In the similar fashion, the array of parallel spring alignment is discussed and following relation is obtained by noticing that the depression ζ_p is determined under $a/r_1 << 1$ and $a/r_2 << 1$.

$$\sigma = \frac{\pi u r_2 E_r}{6 t_2}\left[3 r_2 \cos(2\theta_m) - 4\lambda\cos^3\theta_m + r_2 - 4 r_1 + 4\delta - 4\left\{(r_1^2 - \lambda^2\sin^2\theta_m)^{3/2} - r_1^3\right\}/\lambda^2\right] \qquad (10)$$

Equations (2), (9), (10) are utilized to calculate δ versus σ characteristics shown by the symbols a, b and c in Fig.6. In the calculation, physical parameters are such that r_1=12.7[mm], E_r=1.3[Pa] and ν_r=0.50 [9]. The curve a is concerned with concave layer extending infinitely with radius r_2=16.75[mm]. The curves b1 and c1 are concerned with thin layers, i.e. t_2=5.8[mm] (r_2=15.0[mm]). The curves b2 and c2 are concerned with thick layers, i.e. t_2=9.3[mm] (r_2=18.5[mm]). The constant u is supposed to be 10.0. From the figure we can say that curves b1 and b2 have high-fidelity as compared with the curves c1 and c2. Such unexpected discovery was made that thinner layer sinks more than thicker layer. This is understood by noticing that the ball is same in size, but different in radius r_2 since the spherical shell is same in size except the curve a. Contact area might become small so that the ball can sink deeper when r_2 becomes greater in a same ball load. The curves b1 and b2 will move closer to the curve a by assigning smaller value to the constant u. From these data we can confirm that our spring models are effective to introduce thickness of the elastic layer. Particularly, the radial alignment spring model is more suitable than the parallel alignment model. Above discussions are related to rigid ball type. Formulations related to the sensor of elastic ball type are also performed in the same way and similar things are said.

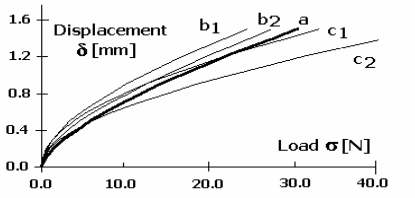

Figure6: Comparison of different models

3. Fabrication of layer and grasping of its physical properties

3.1 Fabrication of the elastic layer

Elastic layers are desired to be uniform to deform against external force from any direction and to respond quickly to force without residual strain (hysteresis). We made spherically formed elastic layers to settle at interior of a spherical shell of diameter around 50[mm]. Material of the layer is a two-component type RTV(Acronym of Room Temperature Vulcanizing) rubber that is commercially available. We use a pair of hemispherical shells of different size as molding template to construct the layer in a concentric configuration. Some other gauges and fixtures are necessary to adjust and keep the gap between the two shells constant before pouring rubber material mixed with catalysis. Inner surfaces of the gap are sprayed by tear off material for easiness of separation. We keep these tools quiet several hours to solidify the material in the normal temperature. Layers referred before are products of this make-up.

Figure7: Fabricated layers

In fact, the test pieces R1, R2, R3 are orange-colored, gray-colored, colorless hemispheres solidified by the materials 165-11MR (Agsa-Japan Co. Ltd.), Rhodorsil RTV-573 (Rhodia Japan Ltd.), KE103RTV (Shin-Etsu Chemical Co., Ltd.) to have E_r=1.1, 1.3, 1.8, respectively. All of these are two-component RTV silicone rubbers. Hardness of these is estimated as 17,18,20, respectively. Poisson's ratio of all products is almost 0.50. Thickness (=t_2) of these pieces is divided into two, i.e. 5.8[mm] and 9.3[mm]. Fig.7 shows these products. The lower part objects in the figure show hemispherical shells of r_2=24.3[mm] and metallic ball of r_1=12.7[mm] for the use in fundamental make-up and experiments. Two hemispherical shells are combined delicately by a fringy groove to make a spherical shell after settling two hemispherical layers inside with a metallic ball. Assembled sensor head is overviewed in Fig.8.

Figure8: spherical sensor head

3.2 Grasping of physical properties

We devised the stand shown in Fig.9 to measure the depression the test pieces. Generally, the stand scale gives total weight and a mechanical micro gauge uses a spring to measure the displacement of its tactile probe. Therefore, true values of δ and σ are calculated from the equation

$$\sigma = Q - L_o + (L_1 + L_2 + L_3) \qquad (11)$$

$$\delta = \delta_g + \delta_o \qquad (12)$$

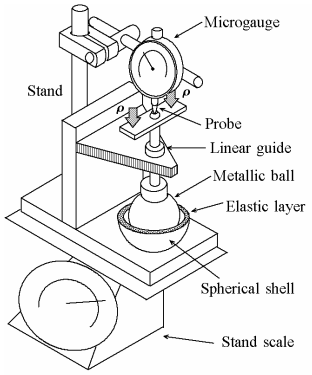

Figure9: Detection of sink

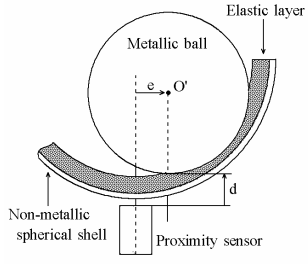

Figure10: Parameters α and β

where δ_o; maximal depression when the layer supports only the ball weight, δ_g; displacement read from the gauge indicator, Q; weight given by the stand scale indicator, L_0; total weight of the apparatuses on the stand scale including micro gauge, L_1; weight of the metallic ball, L_2; weight of enclosures between the probe and ball, L_3; force to drive the micro gauge. Steady depression δ_o might be given by using laser range sensor in advance. L_3 is peculiar to the gauge and given as a function of its probe displacement. External force ρ in Fig.9 augments the value of σ. Experimental data of δ versus σ characteristics of the test pieces are already shown in Fig.4. The data imply that the material R2 is the best in the three to make range of depression wide.

4. CALCULATION OF THE METALLIC BALL POSITION

4.1 Estimation of the ball surface based on sensor signal

In order to collect information for determining ball center in the shell, we use proximity sensors of high-frequency oscillation type, E2CA-X5A, OMRON Corp.[10]. This is sensitive to metallic objects in the range 0-5[mm]. The sensor is symmetric with respect to the axis and produces current proportional to the distance of the front metal, but the distance is a mixture of the parameters of d and e(see Fig.10). Therefore the current is not enough to show where the ball is. It shows only a curved surface with which the ball contacts. Fig.11 shows the surface generated depending on the output current by the sensor S_i. Evidently, the surface is expressed as an ellipsoid of rotation when the sensor faces the center of the shell. Advance preparation makes it possible to get function for determining the surface uniquely by the amount of the current.

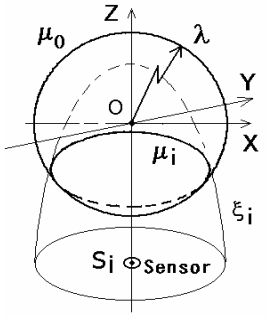

Figure11: Ellipsoid of rotation

4.2 Calculation of the ball center position in 3-D space

Notice that the possible curved contacting surface for tracking the ball is given when the proximity sensor gives a certain value. The surface is simply translated toward the center of the shell with the amount r_1 to produce new but analogous surface [5]. Fig.11 makes it sure that possible ball center area exists on the new curved surface, say ξ_i concerned with the sensor S_i. We call the new surface a *profile* of the ball center.

Since our sensor head is attached on a slow motion object, the ball moves by rolling on elastic layer without jumping. Therefore, the ball center exists on surface of a sphere having radius λ expressed by (8) (see Fig.11). The surface, say μ_o, crosses with the surface ξ_i to have the circle, say μ_i. Fig.12 shows that the μ_i (i=1-3) meet together at a point O'. This is true in algebraic point view, but it might be hard to find the point in numerical processing. Therefore, we determine the position O' as the point that makes the sum of distances to the three circles minimal. In particular, in our orthogonal arrangement of the proximity sensors shown in Fig.12, the sectional coordinate of the sphere with the profiles ξ_i(i=1-3), say (V_1,V_2,V_3) stand for the coordinates O'(x, y, z). This is quite beneficial to determine the ball center position in a simple manner.

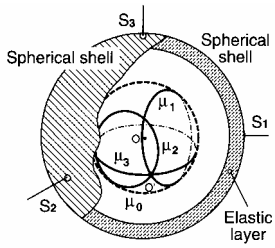

Figure12: Common point among ellipsoids μ_o, μ_1, μ_2, μ_3

5. ASSEMBLY AND EXPERIMENTS

5.1 Assembly of the sensor head as a sensing device

The sensor head in Fig.8 is composed with an steel ball of radius 17.5 [mm] and weight 1.71[N], elastic layer of R2 (25.5,19.5,6.0), acrylic shell of inner radius 25.5 [mm]. The shell is hollowed out from an acrylic rectangular by a NC lathe. Fig.13 shows electric wire connections. To make the sensor head incline in all directions, we use a 2-DOF motion simulator for changing angles of α and β, corresponding to longitude and latitude, respectively. The sensor head fixed on the simulator is overviewed with amplifiers in Fig.14. Sensor probes are little bit longer.

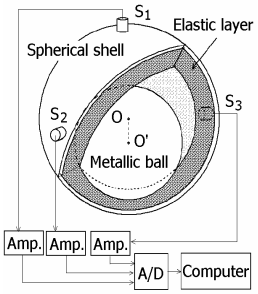

Figure13: Signal

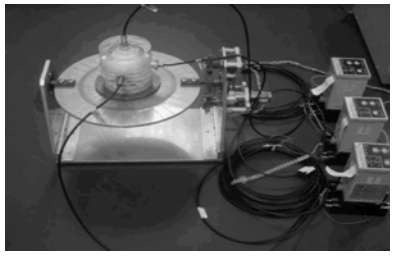

Figure14: Overview of the experimental set with three amplifiers

5.2 Experiment

Outputs of the three proximity sensors are transferred to PC for extracting acceleration. Two axes of the simulator are rotated to change randomly the angles of α and β with an increment of $\pi/9$, $\pi/6$[rad]. Suppose that these angles designate directions toward which the elastic layer depresses at most. These directions are depicted with circles on

grids in Fig.15. Blackened circles show experimental results. In addition, size of the blackened circle is proportional to the magnitude of acceleration. Left and right figures show the data close to equator and to South Pole, respectively. Ranges of α and β are $-\pi \leq \alpha[\text{rad}] \leq \pi$ and $-\pi/2 \leq \beta[\text{rad}] \leq \pi/2$. We collected experimental data three times per one designated data with step angles $\pi/9$ or $\pi/6$[rad]. Ideal results are same in size with the circles at grid points. Brim and bed areas of the shell are shown in left and right. Evidently, the experimental data are in the vicinity of the designated data. This proves that the spherical sensor is useful for all direction measurement. Also, it is confirmed that the error of the acceleration measurement is less than ± 7.4[deg] and 2.86×10^{-2}[m/s^2]. With respect to angular error in a steady state, it became clear that harder rubber and bigger ball make the error small.

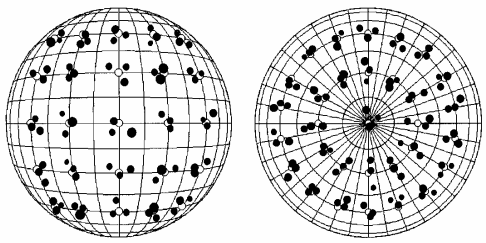

Figure15: Results of the acceleration measurement(π/18 rad/div.)

6. CONCLUSION

We proposed an acceleration sensor using a spherical shell with a metallic ball and an elastic layer. Orthogonal aligning of the three proximity sensors and integration of the sensor outputs made it possible to measure resultant acceleration with results such that angular error less than ± 7.4[deg], amount error less than 2.86×10^{-2}[m/s^2], force sensitivity 4.9×10^{-2}[N], insensible range less than ± 3.8[deg] and periodic time 95[ms]. These results are not high in accuracy, but good for sensing balance of moving objects in all directions in 3-D space, specifically for the application to the robot moving slowly in pipe, for instance.

ACKNOWLEDGEMENTS

This study was supported in part by the Grant-in-Aid for Scientific Research (C2-14550413), the Grant of Mitsutoyo Association for Science and Technology (MAST), and also the Scholarship of the Alexander von Humboldt Foundation.

REFERENCES

[1] Bau H.H., Rooji N.F., Kloeck B., Mechanical sensors (Capacitive microaccelerometers), Sensors, **7**, 1993, pp.125-144

[2] Rouff M. and Konieczka S., Intelligent sensors for force and weight measurement using mechatronic technology, *Proc. of the IECON'93*, 1993, pp.1522-152

[3] Katagiri Y., Itao K., Dynamic microforce measurement by distortion detection with a coupled-cavity laser displacement sensor stabilized in a mechanical negative-feedback loop, Applied Optics, **37**-31, 1998, pp.7193-7199

[4] Microstone Co. Ltd., Brochure of mini-sized 3-axis acceleration sensors, http://www.microstone.co.jp

[5] Okada T., Suzuki N., Kurosaki K., Direction measurement of acceleration in 3-D space based on sensing a metallic ball position in a spherical shell, *Trans.SICE of Japan*. **40**-12, 2004, pp.10-17

[6] Sakamoto M., Zhu Q.-F., Hara T., Shibuya T., Axisymmetric indentation of a transversely isotropic layer by a rigid sphere, *Theo. Appl. Mech.*, **45**, 1996, pp.39-49

[7] Ishibashi T., Sukigara S., et al., Indentation theory of the round tip triangular pyramidal indenter neglecting elastic deformation of the indenter's holding part, *J.Mater.Test. Res.* **45**-3, 2000,pp.426-434

[8] Strength design databook , Japan, Shoukabou Press Ltd., 1968, p.1077-1091

[9] Kubo R., Rubber Elasticity, 2nd ed., Japan, Shoukabou Press Ltd., 1996, pp. 7-9, 76-80

[10] OMRON Corporation, Data of the linear proximity sensor E2CA-X5R, Catalogue page, 1996 - 2004, http://www.fa.omron.co.jp/data_pdf/cat/e2ca_web.pdf

Addresses of the Authors:

Tokuji Okada, Measurement of resultant acceleration utilizing a weight ball rolling in a spherical shell, Niigata University, Faculty of Engineering, Ikarashi 2-8050, Niigata, P.O. Box: 950-2181, Japan, okada@bc.niigata-u.ac.jp